Journal of proteome research

Article

pubs.acs.org/jpr

NMR Metabolomics Show Evidence for Mitochondrial Oxidative Stress in a Mouse Model of Polycystic Ovary Syndrome

Ebru Selin Selen,[†] Zeinab Bolandnazar,[†] Marco Tonelli,[‡] Daniel E. Bütz,[§] Julia A. Haviland,[†] Warren P. Porter,[†] and Fariba M. Assadi-Porter*[,†,‡]

[†]Department of Zoology, [‡]Magnetic Resonance Facility at Madison, and [§]Department of Animal Sciences, University of Wisconsin-Madison, Madison, Wisconsin 53706, United States

Supporting Information

ABSTRACT: Polycystic ovary syndrome (PCOS) is associated with metabolic and endocrine disorders in women of reproductive age. The etiology of PCOS is still unknown. Mice prenatally treated with glucocorticoids exhibit metabolic disturbances that are similar to those seen in women with PCOS. We used an untargeted nuclear magnetic resonance (NMR)-based metabolomics approach to understand the metabolic changes occurring in the plasma and kidney over time in female glucocorticoid-treated (GC-treated) mice. There are significant changes in plasma amino acid levels (valine, tyrosine, and proline) and their intermediates (2-hydroxybutyrate, 4-aminobutyrate, and taurine), whereas in kidneys, the TCA cycle metabolism (citrate, fumarate, and succinate) and the pentose phosphate (PP) pathway products (inosine and uracil) are significantly altered ($p < 0.05$) from 8 to 16 weeks of age. Levels of NADH, NAD^+, NAD^+/NADH, and NADH redox in kidneys indicate increased mitochondrial oxidative stress from 8 to 16 weeks in GC-treated mice. These results indicate that altered metabolic substrates in the plasma and kidneys of treated mice are associated with altered amino acid metabolism, increased cytoplasmic PP, and increased mitochondrial activity, leading to a more oxidized state. This study identifies biomarkers associated with metabolic dysfunction in kidney mitochondria of a prenatal gluococorticoid-treated mouse model of PCOS that may be used as early predictive biomarkers of oxidative stress in the PCOS metabolic disorder in women.

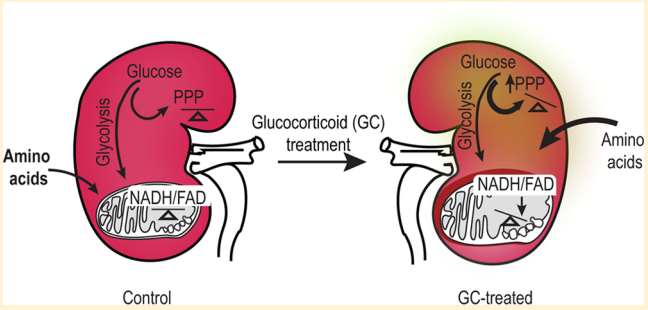

KEYWORDS: *polycystic ovary syndrome (PCOS), animal model, metabolomics, nuclear magnetic resonance (NMR), oxidative stress, mitochondria*

1. INTRODUCTION

Polycystic ovary syndrome (PCOS) is an endocrine disorder in women of reproductive age with a prevalence of 10−20%[1−3] and is associated with complex metabolic pathologies.[4] Despite the unknown origin of onset in PCOS, a number of factors, such as environmental, (epi)-genetic, and hormonal influences, are thought to be important in the development of this syndrome. PCOS exhibits at puberty with multiple phenotypes[5,6] as characterized by NIH criteria: androgen excess, ovulatory dysfunction, and polycystic ovaries.[7] Type 2 diabetes (T2D), hyperandrogenism, cardiovascular diseases, an unusual increase in lipid synthesis, and induced weight gain and obesity are common metabolic syndromes associated with PCOS.[4,8,9] Thus, early diagnosis of PCOS is crucial for influencing the overall life quality of women with PCOS.

Kidney tissue has been shown to play roles in maintaining glucose homeostasis,[10] amino acid metabolism, ammonia production, interorgan exchange of nitrogenous metabolites,[11,12] and clearance and synthesis of lipid binding proteins and regulatory hormones.[13] Recently, a kidney denervation process has been suggested for ameliorating the components of PCOS, such as elevated blood glucose levels, insulin sensitivity, glomerular hyperfiltration, and microalbuminuria[14] in obese PCOS patients. Research suggests that kidney tissues may be a promising target for understanding PCOS metabolic dysfunction.

Metabolomics is widely used to monitor major alterations in metabolism and measure fingerprints of disease onset and progression stages. Untargeted one-dimensional (1D) ^{1}H NMR-based metabolomics provides information about overall metabolic changes in biological tissues. We have previously demonstrated by 1D ^{1}H NMR-based metabolomics studies that women with PCOS exhibit significant dysfunction in carbohydrate and lipid metabolism, and utilization of amino acids as the preferential carbon source is one of the significant differences between healthy women and women with PCOS.[15]

Glucose is the major substrate that is normally catabolized through a series of cytosolic (glycolysis) and mitochondrial (TCA cycle) reactions to produce ATP as a major cellular energy source.[16] During the sequential reactions, nicotinamide adenine dinucleotide (NAD^+, NADH) and flavin adenine

Received: April 10, 2015
Published: June 16, 2015

DOI: 10.1021/acs.jproteome.5b00307
J. Proteome Res. 2015, 14, 3284−3291

Table 1. Total Cellular NADH, NAD^+, NAD^+/NADH, and Mitochondrial Redox Ratio (NADH/FAD) Measurements in the Kidney Tissues of GC-Treated and Control Mice at All Time Points

age[a]	treatment[b]	NADH	NAD^+	NAD^+/NADH	NADH/FAD
8W	C	78819.5 ± 3195.8	118484.3 ± 2959.6	1.511 ± 0.047	1.725 ± 0.1332
	GC	89102.2 ± 750.4[c]	125650.3 ± 4445.2	1.411 ± 0.054	0.867 ± 0.0815[c]
12W	C	83241.2 ± 3866.9	118458.7 ± 3248.1	1.437 ± 0.067	2.07 ± 0.3737
	GC	85915 ± 1281.7	122634.2 ± 3780.3	1.429 ± 0.049	1.760 ± 0.2814
16W	C	88560.3 ± 1896.8	129301.8 ± 5585.2	1.459 ± 0.055	1.867 ± 0.0133
	GC	64393.7 ± 11052.8[d]	102060.3 ± 14017.4	1.681 ± 0.149	1.587 ± 0.0211[c]

[a]8W, 8 weeks old; 12W, 12 weeks old; 16W, 16 weeks old. [b]C = control mice, and GC = GC-treated mice. [c]Indicates $p < 0.05$. [d]Indicates $p < 0.1$.

dinucleotide (FAD^{2+}, FADH2) serve as major oxidizing and reducing substrates in the production of ATP. NADH is oxidized to NAD^+ mainly through oxidative phosphorylation in the mitochondria and has a negligible contribution from NADH and NAD^+ generated in the cytosol.[17] These molecules are important cofactors in catabolic processes[18] and are sensitive to mitochondrial anomalies and cellular redox reactions.[19] The redox ratio of the fluorescence intensity of fluorophores NADH/FAD, also known as the optical redox ratio) was previously shown as a marker of the cellular redox state that is sensitive to anabolic or catabolic conditions (i.e., mitochondrial energy production and/or mitochondrial oxidative stress as well as lipid metabolism) in cells or tissues.[17,20−22] Significant alterations in the optical redox ratio have been shown to be a differentiation factor in cancer cell studies,[23−25] virus infection,[26] stem cell differentiation,[17] and metabolic studies.[27]

In this study, we used untargeted NMR-based metabolomics to obtain an overview of possible metabolic pathway changes in kidney and plasma metabolome profiles in a prenatal glucocorticoid (GC)-treated mouse model of PCOS as previously described.[28] GC-treated mice showed greater metabolic changes with milder phenotypic changes in their mating and estrous cycles (i.e., earlier vaginal opening, reduced estrous cycles, and less parturition compared to those of control group animals (Supporting Information (SI), Figure S1). These changes are consistent with the widely used PCOS animal models, which were exposed to prenatal or neonatal androgen[29−33] and estradiol valerate.[34−36]

Among a variety of prenatally administered sex-steroid hormones, prenatal cortisol treatment in mice exhibits a mild version of metabolic dysfunction in the female offspring similar to those observed in women with PCOS.[28,37] On the basis of our previous data, we hypothesized that increased glucose flux toward the TCA cycle and pentose phosphate (PP) pathway results in an altered redox state in mitochondria, which has been shown to lead to a number of reproductive disturbances, such as infertility and endometriosis in women with PCOS.[38]

Our results show that amino acid intermediates in plasma, and in PP and TCA cycle intermediates in the kidney, are differentiating factors between GC-treated and control mice. In addition, metabolic changes coincide with an altered mitochondrial redox ratio (RR) in GC-treated mice, which indicates mitochondrial metabolism is another important feature in this mouse model of PCOS.

2. MATERIALS AND METHODS

2.1. Animal Study

All animal procedures were approved by the University of Wisconsin, College of Letters and Science, Animal Care and Use Committee (Madison, WI). Ten CD-1 breeding pairs of mice were obtained from Harlan (Indianapolis, IN). Mice were fed an AIN-93G diet (17.7% protein, 60.1% carbohydrate, and 7.2% fat) (Harlan, Indianapolis, IN) and water ad libitum under normal housing conditions. All mice were allowed to acclimate for 2−3 weeks before mating. The procedure for GC-treated dams was followed according to our previous publication.[28] Dams were randomly injected subcutaneously with either 6α-hydroxycortisol dissolved in ethanol (1.9 mg kg^{-1} day^{-1}; 1:9 v/v; GC-treated; $n = 5−9$) in a certified organic sesame oil carrier or carrier alone (control; $n = 5$) on GD 16 through GD 19 as previously described.[28] F1 generation female mice were randomly grouped after weaning for metabolic progression studies. There was no weight difference between GC and control groups. Changes in phenotypes in GC-treated mice were measured by vaginal opening, reduced estrous cycles, and less female parturition compared to those of control group animals (SI, Figure S1). Kidney tissues were removed from GC-treated and age-weight matched control females at 8, 12, and 16 weeks of age, flash frozen in liquid nitrogen, and kept at −80 °C until further use.

2.2. NMR Tissue Sample Preparation

Kidney tissue samples were thawed on ice. Individual 50 mg tissue samples were placed on ice in 10 mM phosphate buffer followed by homogenization by an Omni Bead Ruptor Homogenizer (Omni International Inc., Waterbury, CT) for 3 min. Homogenized tissues were transferred to new 2 mL Eppendorf tubes and were centrifuged for 10 min at 5,000 *g*. The supernatant was then transferred to a new 2 mL tube, and ice-cold methanol (2:1, v/v) was quickly added to aliquots of the supernatants, and the tubes were then vortexed for 30 s to enhance protein precipitation followed by cooling to −20 °C for 30 min. After a precipitation period, the tubes were vortexed once more for 10 s and centrifuged at 5,000*g* for 10 min. The supernatant was dried in a speed vacuum overnight. The dried supernatant was then reconstituted in the NMR buffer and adjusted to pH 7.4 ± 0.05.

2.3. NMR Data Collection, Metabolite Detection, and Quantification

All 1D ^{1}H NMR spectra were collected at 25 °C on a 600 MHz Varian VNMRS spectrometer equipped with a cryogenic probe according to our previously published method.[28] Each 1D spectrum was accumulated for 1028 scans with an acquisition time of ∼2.5s (25,000 complex points) and a 3 s repetition delay for a total collection time of ∼2 h.[28] 1D ^{1}H NMR spectra were referenced to 0.5 mM 4,4-dimethyl-4-silapentane-1-sulfonic acid (DSS). NMR signals arising from small metabolites (<1000 Da) were identified and quantified relative to formate (1 mM) as the internal reference by Chenomx

DOI: 10.1021/acs.jproteome.5b00307
J. Proteome Res. 2015, 14, 3284−3291

software version 6 (http://www.chenomx.com). All metabolite concentrations are reported as values relative to formate.

2.4. NAD+, NADH, and Mitochondrial RR Measurements

Total abundance of cellular oxidized and reduced nicotinamide adenine dinucleotides, NAD^+, and NADH and their ratio in kidney samples were determined by an NAD^+/NADH Glo assay kit (Promega, Madison, WI). Sample preparation and final calculations were performed according to the manufacturer's instructions. Sample preparation and measurements for the NADH/FAD (or mitochondria RR) were performed as previously described.[22,39] Measurements of NAD^+, NADH, NAD^+/NADH, and NADH/FAD are presented as the mean ± SEM of experimental duplicates (n = 3 per group; Table 1). The Student's t test was used to detect significance; $p < 0.05$ was considered statistically significant, and $p < 0.1$ was considered moderately significant.

2.5. NMR Data Analysis

Log transformed ($\log_2$) data were used in all statistical procedures. Data were pretreated with Pareto scaling before the t test was used to assess the significance of changes between PCOS and control groups. The t test results are provided in SI Table S1. Individual profiled metabolite levels are presented in SI Figure S2A–C as individual cells in the heatmap. The heatmap and clustering analysis were applied using a Euclidian distant metric and ward clustering method[40] to calculate the clusters of GC-treated and control groups (SI, Figure S2A–C). MetaboAnalyst (http://www.metaboanalyst.ca/)[41] was used to generate the clustering and heatmaps.

The t test and fold change heatmaps were computed as the ratio of $\log_2$ transformed concentration of metabolites of PCOS to control values using R (http://www.R-project.org). Complete fold changes of kidney and plasma metabolome profiles are provided in SI Tables S2 and S3. Changes that have p values lower than 0.05 ($p < 0.05$) were considered significant, whereas p values between 0.1 and 0.05 ($p < 0.1$) were considered moderately significant. Data are reported ± SEM.

3. RESULTS

3.1. 1D ^{1}H NMR Metabolomics of Plasma and Kidney Tissues

A total of 30 metabolites in the plasma and 40 metabolites in the kidney were identified and quantified. In the plasma metabolome profile, 60.6% of the identified metabolites are intermediates in amino acid metabolism, 21.2% involve primarily lipid metabolism, and 18.2% are involved in energy production pathways, such as glycolysis and the TCA cycle (Figure 1A). In the kidney metabolome profile, 50% of the profiled metabolites are amino acids, 17.5% are primarily lipid metabolism intermediates, 15% are involved in energy production pathways, 15% are sugar nucleotides, and 2.5% are antioxidant metabolism intermediates (Figure 1B).

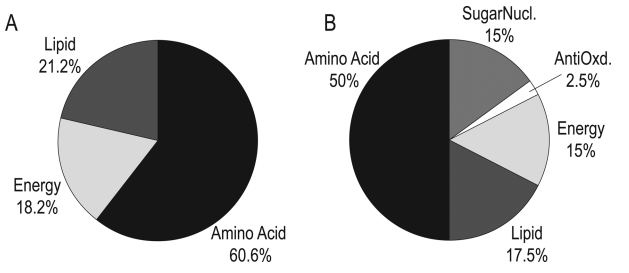

Figure 1. Tissue-specific metabolite contents of (A) plasma and (B) kidney metabolome. Abbreviations: SugarNucl, Sugar Nucleotides; AntiOxd, Antioxidant.

3.2. Significant Changes Are Detected in the Plasma Lipid and Amino Acid Metabolic Profiles between GC-Treated and Control Mice at Eight and 16 Weeks of Age

Figure 2A shows a heatmap of fold changes in the identified metabolites in plasma. Fold change values are shown in SI Table S2. A total of eight metabolites in the plasma of eight and 16 week old mice are significantly different between GC-treated and control mice. In the eight-week old GC-treated mice, the nitrogen metabolism intermediate creatine level is significantly increased compared to the control ($p < 0.05$). The creatinine level is higher ($p < 0.1$), whereas the choline level is lower ($p < 0.1$), in eight-week old GC-treated mice compared to those of control mice.

Between the 12-week old mice, acetate ($p < 0.05$), tyrosine ($p < 0.05$), and valine ($p < 0.1$) concentration levels are significantly decreased in GC-treated plasma (Figure 2A).

Comparison of 16W old mice plasma metabolome profiles shows that the antioxidant intermediate 2-amino butyrate (2AB) and several amino acid metabolic intermediate levels, including 4-aminobutyrate (4-AB), phenylacetate (Phelact), creatinine, and proline, are significantly ($p < 0.05$) reduced in GC-treated mice (Figure 2A and 3A). In addition, the level of taurine is also reduced ($p < 0.1$) in the 16-week old GC-treated mice compared to that of the control mice.

3.3. Significant Changes in TCA and Pentose Phosphate Metabolites Concentration Are Detected between GC-Treated and Control Mice at Eight and 16 Weeks in Kidney Tissues

Fold change values and heatmap in the identified metabolites are shown in SI Table S3 and Figure 2B in kidney tissues. The metabolites with the significant differences in fold change in the GC-treated group were mainly associated TCA cycle and PP pathways (Figures 2B and 3B) with trends in increasing/decreasing levels of essential, aromatic, and branched chain amino acids (Figure 2B) across time points.

TCA cycle intermediate (fumarate) and PP metabolism intermediate (uracil and inosine) levels are significantly increased ($p < 0.05$), whereas the level of another PP metabolism intermediate, xanthine, in the 8-week old GC-treated mice is almost significantly lower ($p < 0.1$) than that of control mice (Figures 2B and 3B). No significant changes are observed in metabolome profiles between 12-week old kidneys of GC-treated and control mice. Between the 16-week old control and treated groups, the antioxidant metabolism intermediate 2-HB level is significantly increased in the GC-treated mice ($p < 0.05$) (Figure 2B and 3B). Increases in the levels of five metabolites almost reach significance ($p < 0.1$). Those metabolites include a PP intermediate (uridine), ketone body metabolism intermediates (3-hydroxybutyrate (3-HB) and acetone), a TCA cycle intermediate (citrate), and TCA cycle-linked glutamate metabolism intermediate 4-AB. Significant changes in mitochondrial TCA activities are observed for fumarate (decreasing) and citrate (increasing) transitioning from eight to 16 weeks in GC-treated mice.

DOI: 10.1021/acs.jproteome.5b00307
J. Proteome Res. 2015, 14, 3284–3291

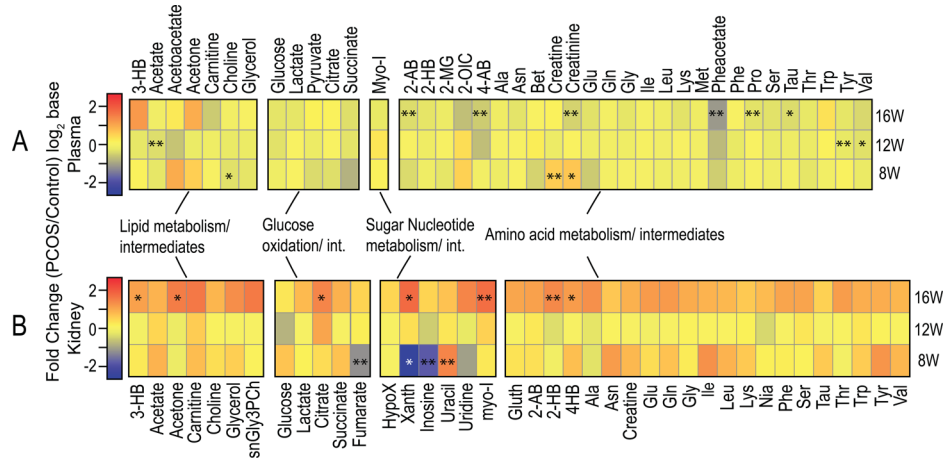

Figure 2. Fold change of all metabolites found in plasma and kidney samples profiled by 1D ^{1}H NMR across time points in (A) plasma and (B) kidneys. Metabolite concentrations were quantified relative to formate. All concentrations were transformed to $\log_2$ base prior to fold changes and Student's *t* test calculations. Fold changes were calculated as the ratio of GC-treated and control groups (GC-treated/control) of a given metabolite for time points of eight weeks of age (8W), 12 weeks of age (12W), and 16 weeks of age (16W) as labeled in the heatmap. Red shows >2 (in $\log_2$ base), and dark blue shows <−2 (in $\log_2$ base). The Student's *t* test was used to evaluate differences in the transformed $\log_2$-based concentration comparison between GC-treated and control mice at a given time period. Double asterisks (**) indicate $p < 0.05$, and single asterisk (*) indicates $p < 0.1$. Abbreviations: 3-HB, 3-Hydroxybutyrate; 2-HB, 2-Hydroxybutyrate; 2-AB, 2-Aminobutyrate; 4-AB, 4-Aminobutyrate; 2-MG, 2-Methylglutarate; 2-OIC, 2-Oxoisocaproate; myo-I, myo-Inositol; Ala, Alanine; Asn, Asparagine; Bet, Betaine; Glu, Glutamate; Gln, Glutamine; Gly, Glycine; Ile, Isoleucine; Leu, Leucine; Lys, Lysine; Met, Methionine; Phe, Phenylalanine; Pro, Proline; Ser, Serine; Tau, Taurine; Thr, Threonine; Trp, Tryptophan; Tyr, Tyrosine; Val, Valine; Nia, Niacinamide; HypoX, Hypoxanthine; Xanth, Xanthine; snGly3PCh, sn-Glycero-3P-Choline.

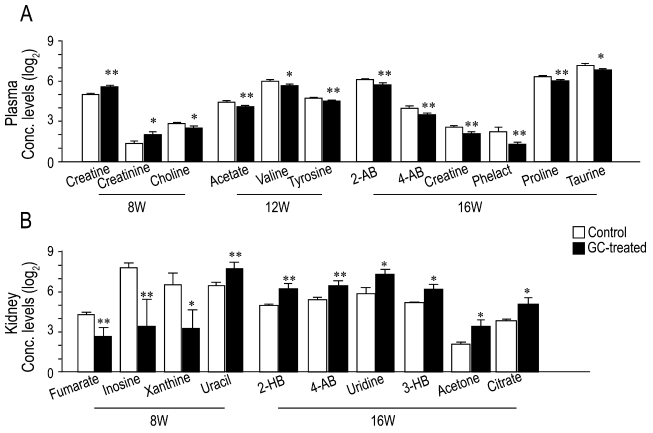

Figure 3. Significantly changed metabolites ($p < 0.05$) detected by Student's *t* test. Significant changes are shown in (A) plasma and (B) kidney metabolome profiles. The outer *x*-axis label shows the time points in weeks (W), the *x*-axis shows metabolites, and the *y*-axis shows $\log_2$ relative concentration levels compared to formate as an internal standard, quantified through 1D ^{1}H NMR. Black bars and white bars represent the GC-treated and control groups, respectively. Double asterisks (**) indicate $p < 0.05$; single asterisk (*) indicates $p < 0.1$. Data are represented as ± SEM values.

3.4. Significant Differences Are Detected in the Mitochondrial Redox State of Eight and 16-Week Old GC-Treated Kidney Tissues

As a complementary test to the kidney metabolome profiles, we measured NADH, NAD$^+$, FAD, and ratios of NAD$^+$/NADH and NADH/FAD as output products for the redox state of mitochondria. We measured total cellular NADH, NAD$^+$, and ratios of NAD$^+$/NADH and NADH/FAD (Table 1).

Total NADH level in the GC-treated mice at eight weeks are significantly higher ($p < 0.05$) than in the controls, but they drop at 12 and 16 weeks ($p < 0.1$), indicating lower available NADH as a reducing agent in the GC-treated mice.

The ratio of NADH/FAD was previously shown to be a reporter of mitochondrial oxidation state in the tissue.[22] The ratio of NADH/FAD is also significantly lower ($p < 0.05$) in eight- and 16-week old GC-treated mice compared to those of the control (Table 1). There is a more oxidized cellular environment in the GC-treated group at later time points. However, levels of NAD$^+$ and ratios of NAD$^+$/NADH (cytosolic reducing state) are comparable across time points in both GC-treated and control mice.

The NADH/FAD ratio is increased by 2-fold from eight to 12 weeks and remains high at 16 weeks within the GC-treated mice, whereas this ratio is not changed across all time points in control mice, suggesting a fundamental difference in the redox state of mitochondria in the GC-treated group.

4. DISCUSSION

PCOS is a complex disease that is associated with hormonal and metabolic syndromes[15] and appears to manifest at puberty with multiple phenotypes.[6,42] In this study, we used a prenatal glucocorticoid treatment in mice to generate a model system with PCOS-like metabolic symptoms[28] that resembles similarities to women with PCOS[15,28] but with milder effects on the reproductive system (SI, Figure S1), to compare metabolic phenotypes of GC-treated animals to women with PCOS. Our previous untargeted metabolome profiling studies of women with PCOS with no apparent type 2 diabetes indicated significant changes in TCA (citrate) and amino acid metabolism, indicating diminished lipid oxidation and possibly increased lipid synthesis in addition to dysfunctional glucose metabolism.[15] Consistent with the studies on women with PCOS, targeted plasma metabolic profiles of GC-treated animals at >20 weeks of age showed significant increases in fluxes of PP and TCA cycle pathways that indicated increased

DOI: 10.1021/acs.jproteome.5b00307
J. Proteome Res. 2015, 14, 3284−3291

fatty acid synthesis in addition to decreased lipid oxidation.[28] However, it is not clear at what time point these metabolic changes take place or how the kidney functions under stressed metabolic activities. This study focuses on screening metabolic markers in plasma for changes in amino acids, glycolysis, and the role of these pathways on mitochondrial activity in kidneys at different time points (8−16 weeks) in the GC-treated mice.

Amino acid metabolism intermediates have a wide variety of roles from being basic substrates for energy production and anabolic processes to being regulators of gene expression and protein phosphorylation.[11,43] Significant deviations from the normal physiological concentrations of amino acids may develop or contribute to pathogenic states, such as neurological disorders, oxidative stress, cardiovascular diseases,[43] as well as metabolic disturbances, such as type 2 diabetes, obesity, and insulin resistance.[44,45] Therefore, an optimal balance of amino acids in circulation is crucial for whole body homeostasis. The kidney is a key organ in the regulation of nitrogen metabolism. It plays a key role in maintaining plasma amino acid concentrations and acid−base homeostasis.[46] In our study, most of the plasma amino acid levels tended to remain lower in the GC-treated mice compared to those of the control mice at all time points (Figure 2A), whereas several of these amino acids (tyrosine, valine, phenylacetate, proline, and 4-AB) are significantly reduced in the GC-treated mice, indicating perturbed amino acid metabolism. This observation is consistent with our previous report on women with PCOS that indicated increased amino acid utilization as a major carbon source for daily energy metabolism in women with PCOS.[15] In addition, other metabolomics reports also showed similar changes in circulating plasma amino acid profiles in women with PCOS with different genetic backgrounds.[47,48]

In contrast to decreased plasma amino acids, the kidney metabolome in GC-treated mice shows higher amino acid levels across all age groups (Figure 2B). Altered amino acid levels suggest that one or more steps in amino acid metabolism, such as uptake, degradation, synthesis and/or release of amino acids. are affected in the GC-treated kidney.

The PP pathway carries on an essential intersecting role in cellular metabolism by providing basic substrates for nucleotide, nucleic acid, and aromatic amino acid synthesis[49] by generating reduced electron carrier nicotinamide adenine dinucleotide phosphate (NADPH) for anabolic reactions, such as lipid synthesis, and for the action of antioxidants and redox regulatory enzymes.[50−52] Under pathological conditions, increased PP has been shown to affect acid/base, electrolyte balances, and protein synthesis rates[53−55] in the kidney. At eight weeks of age, GC-treated mice show significant decreases in purine level intermediates (inosine and its oxidized product xanthine; Figures 2B and 3B), indicating increased turnover and metabolism to other oxidized molecules. One consequence of the increased catabolism of purines is the formation of uric acid as an end waste product through one of the reactive oxygen species, generating reactions catalyzed by xanthine oxidase (XO).[56] Induced XO activity is associated with renal hemodynamic and reabsorption anomalies[57] and renal injuries in hyperlipidemia. The latter syndrome is commonly associated with PCOS in women. [58]

Metabolome analysis in kidneys shows a significant increase in PP in GC-treated compared to control mice, which affects the cellular redox state leading to metabolic stress. In the 16-week old GC-treated mice, PP intermediates are at relatively higher levels than the corresponding control group (Figures 2B and 3B). These results are supported by our previous studies in the same PCOS animal model system of >20 week old mice, which indicated a 29−33% increased flux through enzymatic pathways of PP and TCA in order to meet the high demand for substrates necessary for downstream lipid synthesis.[28] One of the major functions of PP is to generate NADPH as a reducing agent that is utilized in anabolic reactions and in antioxidant activities.[59] Therefore, PP plays an important role in maintaining cellular redox homeostasis.[50] Major alterations in the PP pathway and TCA cycle intermediates provide further evidence for altered metabolism and oxidation states in mitochondria of GC-treated mice as early as eight weeks after beginning treatment and continuing through later time points.

The mitochondrial electron transport system (ETS) consists of five enzyme complexes, complexes I−IV and ATP synthase,[60] which carry out oxidative phosphorylation, produce energy in the form of ATP, and maintain oxidation/reduction processes in the mitochondria. Four of the ETS enzymes, complexes I−IV, and their interactions are shown in Figure 4A.

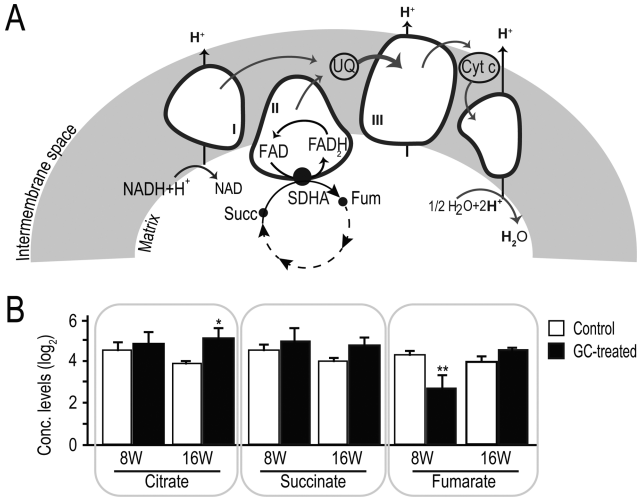

Figure 4. Kidney metabolome schematics representing metabolomics pathways for metabolome data, indicating disruption in mitochondrial metabolism through TCA-ETS substrate flow. (A) Schematic of the ETS complexes and their biochemical connections to paths in the TCA cycle. Succinate and fumarate are also linked to the ETS through a subunit of complex II, succinate dehydrogenase A (SDHA), which catalyzes the oxidation reaction of succinate to fumarate. (B) The panel shows relative $\log_2$ transformed concentration levels of TCA cycle substrates, citrate, succinate, and fumarate. The *x*-axis shows the time points in weeks (W), and the *x*-axis labels list the metabolites. The *y*-axis shows the $\log_2$ transformed relative concentration levels compared to formate as an internal standard as quantified through 1D ^{1}H NMR. Black and white bars represent the GC-treated and control groups, respectively. The Student's *t* test was used to evaluate the data. Double asterisks (**) indicate $p < 0.05$; single asterisk (*) indicates $p < 0.1$. Data are represented as ± SEM values.

Complex I of the ETS is the first step in the mitochondria that converts NADH to NAD^+ (Figure 4A). Complex II (succinate dehydrogenase (SDH)) catalyzes an electron transfer from succinate to ubiquinone via flavin adenine dinucleotide (FAD) as an essential cofactor.[61] Furthermore, the Subunit A of SDH (SDHA) enzyme in the TCA cycle plays an important role in the conversion of succinate (Succ) to fumarate (Fum) (Figure 4). Metabolome data provides further evidence for the increase in citrate, fumarate, and succinate (TCA cycle intermediates)

DOI: 10.1021/acs.jproteome.5b00307
J. Proteome Res. 2015, 14, 3284−3291

levels from eight to 16-weeks (Figure 4B) in the GC-treated group. Because of the involvement of these complexes in carrying reactions in metabolic pathways, NAD^+/NADH and NADH/FAD ratios are important indicators of the cellular redox state.[62,63]

The redox ratio of NADH/FAD is inversely proportional to the cellular metabolic rate[17,64,65] and is sensitive to the balance between glucose consumption and ATP production.[17] Changes in NADH/FAD RRs are shown to be an indicator of increased oxidative phosphorylation to supply higher ATP demand[63] or indicate increased mitochondrial oxidative stress.[39] Our study shows that the mitochondrial redox state NADH/FAD in GC-treated kidneys is significantly lower by 50% relative to control kidneys at as early as eight weeks of age (Table 1), indicating more oxidative stress in the mitochondria of GC-treated mice. Interestingly, although the NADH/FAD ratio is increased by 2-fold in GC-treated mice from eight to 16 weeks of age, the ratio in GC-treated mice remains significantly lower at 16 weeks than in control mice, indicating a more perturbed metabolism and increased oxidative phosphorylation in mitochondria. It is important to note that the NADH/FAD ratio is not changed in control mice across all ages, indicating more stable kidney metabolism/function.

The ratio of NAD^+/NADH is an important factor that regulates the rate of glycolysis[66] and could contribute to the production of total cellular NAD^+ and NADH levels. Table 1 shows that NAD^+ and the ratio NAD^+/NADH do not act as differentiating factors between GC-treated and control kidneys at all time points. Furthermore, our 1D ^{1}H NMR measurements of glycolytic metabolites (glucose, lactate, and acetate; SI, Figure S3) also suggest that the metabolic alterations in glycolysis are not likely to have an impact on the observed changes in oxidation state and NADH/FAD redox ratios in GC-treated mice. However, an assay-based total cellular NADH measurement shows a significant increase in eight-week old GC-treated mice and then a decrease in the 16-week old GC-treated mice (Table 1), indicating a change in the redox state of mitochondria in the GC-treated group. Because of the inverse proportion of NAD^+ and the amount of substrates in the metabolic reactions, NADH must be rapidly oxidized to avoid any disturbances in the NAD^+ consuming reactions.[18] Changes in NADH levels between GC-treated and control groups may be related to the tissue oxygen levels in GC-treated mice because oxygen serves as the terminal acceptor of the electrons donated by NADH in ETS.[67,68] Additional work is necessary to understand the cause of the changes in total NADH levels.

Mitochondrial-mediated redox imbalance is suggested to be an important step associated with the pathogenesis of several other diseases that also have increased lipogenesis and hyperlipidemia, such as diabetes, nephrotic syndrome, obesity, and metabolic syndrome.[69] Our NMR metabolomics results show significant changes in several pathways; reducing cofactor (NADPH)-generating PP pathway and TCA cycle intermediates are significantly associated with alterations in the kidney tissue redox state in the GC-treated mice. Alternatively, perturbations in amino acid metabolism in the plasma (reduced levels) relative to kidney (increased levels) indicate changes in distribution and carbon metabolism in GC-treated mice that may be linked to the redox imbalance in tissues.

Our results show that the mitochondrial redox ratio (measured by changes in reduced NADH and oxidized FAD) is an important contributing factor differentiating GC-treated from control mice. The combination of the ensemble of mitochondrial markers (NADH, FAD, and TCA cycle intermediates (i.e., citrate and fumarate)) could be used as indicators of metabolic disturbances in lipid metabolism and associated oxidative stress in GC-treated mice. This is the first study to show that mitochondrial metabolic markers may be used as an early predictive biomarker of oxidative stress in women with the PCOS metabolic disorder.

■ ASSOCIATED CONTENT

Supporting Information

Table S1: Student's t test showing significant ($p < 0.05$) and almost significant ($p < 0.1$) alterations in kidney and plasma metabolites between GC-treated and control mice. Table S2: Plasma fold change values of metabolites (GC-treated/control) identified by 1D ^{1}H NMR metabolomics. Table S3: Kidney fold change (GC-treated/control) values of metabolites identified by 1D ^{1}H NMR metabolomics. Figure S1: Measurements of differences in vaginal opening, estrous cycle, and parturition between GC-treated and control groups. Figure S2: Heatmap representation of kidney metabolome profiles. Figure S3: Relative concentrations levels of glycolytic substrates between GC-treated and control groups shown for all time points. The Supporting Information is available free of charge on the ACS Publications website at DOI: 10.1021/acs.jproteome.5b00307.

■ AUTHOR INFORMATION

Corresponding Author

*Phone: +1(608)-262-0029. E-mail: fariba@nmrfam.wisc.edu, fassadiporter@gmail.com.

Notes

The authors declare the following competing financial interests: F.M.A.-P., M.T., D.B., and W.P.P. are cofounders of Isomark LLC. F.M.A.-P. is the founder of Metresponse LLC.

■ ACKNOWLEDGMENTS

This research was supported by NIH Grants R01 DC009018 and RC4 EY021357 and a Wisconsin Institute of Discovery Grant (WID-135A039) to F.M.A.-P. We thank Dr. Cecile Ane for statistical consulting and help, Michael Rogowski and Zahra Ghanian for help with the mitochondrial redox measurements, and Daniel Finn, Chin Tan, and Marisa Schwartz for help with the animal studies.

■ REFERENCES

(1) Knochenhauer, E. S.; Key, T. J.; Kahsar-Miller, M.; Waggoner, W.; Boots, L. R.; Azziz, R. Prevalence of the polycystic ovary syndrome in unselected black and white women of the southeastern United States: a prospective study. *J. Clin. Endocrinol. Metab.* **1998**, *83* (9), 3078−3082.

(2) Fertil Steril. Rotterdam ESHRE/ASRM-Sponsored PCOS Consensus Workshop Group.. Revised 2003 consensus on diagnostic criteria and long-term health risks related to polycystic ovary syndrome (PCOS). *Hum. Reprod.* **2004**, *19* (11), 4006−11.

(3) Diamanti-Kandarakis, E.; Kouli, C. R.; Bergiele, A. T.; Filandra, F. A.; Tsianateli, T. C.; Spina, G. G.; Zapanti, E. D.; Bartzis, M. I. A survey of the polycystic ovary syndrome in the Greek island of Lesbos: hormonal and metabolic profile. *J. Clin. Endocrinol. Metab.* **1999**, *84* (11), 4006−4011.

(4) Giallauria, F.; Orio, F.; Palomba, S.; Lombardi, G.; Colao, A.; Vigorito, C. Cardiovascular risk in women with polycystic ovary syndrome. *J. Cardiovasc. Med.* **2008**, *9* (10), 987−992.

(5) Ewens, K. G.; Stewart, D. R.; Ankener, W.; Urbanek, M.; McAllister, J. M.; Chen, C.; Baig, K. M.; Parker, S. C. J.; Margulies, E.

DOI: 10.1021/acs.jproteome.5b00307
J. Proteome Res. 2015, 14, 3284−3291

H.; Legro, R. S.; Dunaif, A.; Strauss, J. F.; Spielman, R. S. Family-Based Analysis of Candidate Genes for Polycystic Ovary Syndrome. *J. Clin. Endocrinol. Metab.* **2010**, *95* (5), 2306−2315.
(6) Goodarzi, M. O.; Dumesic, D. A.; Chazenbalk, G.; Azziz, R. Polycystic ovary syndrome: etiology, pathogenesis and diagnosis. *Nat. Rev. Endocrinol.* **2011**, *7* (4), 219−231.
(7) Ehrmann, D. A.; Liljenquist, D. R.; Kasza, K.; Azziz, R.; Legro, R. S.; Ghazzi, M. N. Prevalence and predictors of the metabolic syndrome in women with polycystic ovary syndrome. *J. Clin. Endocrinol. Metab.* **2006**, *91* (1), 48−53.
(8) Cascella, T.; Palomba, S.; De Sio, I.; Manguso, F.; Giallauria, F.; De Simone, B.; Tafuri, D.; Lombardi, G.; Colao, A.; Orio, F. Visceral fat is associated with cardiovascular risk in women with polycystic ovary syndrome. *Hum. Reprod.* **2008**, *23* (1), 153−159.
(9) Vinaixa, M.; Rodriguez, M. A.; Samino, S.; Diaz, M.; Beltran, A.; Mallol, R.; Blade, C.; Ibanez, L.; Correig, X.; Yanes, O. Metabolomics reveals reduction of metabolic oxidation in women with polycystic ovary syndrome after pioglitazone-flutamide-metformin polytherapy. *PLoS One* **2011**, *6* (12), e29052.
(10) Mather, A.; Pollock, C. Glucose handling by the kidney. *Kidney Int. Suppl.* **2011**, *120*, S1−6.
(11) van de Poll, M. C.; Soeters, P. B.; Deutz, N. E.; Fearon, K. C.; Dejong, C. H. Renal metabolism of amino acids: its role in interorgan amino acid exchange. *Am. J. Clin. Nutr.* **2004**, *79* (2), 185−197.
(12) Dejong, C. H.; Deutz, N. E.; Soeters, P. B. Ammonia and glutamine metabolism during liver insufficiency: the role of kidney and brain in interorgan nitrogen exchange. *Scand. J. Gastroenterol., Suppl.* **1996**, *218*, 61−77.
(13) Moestrup, S. K.; Nielsen, L. B. The role of the kidney in lipid metabolism. *Curr. Opin. Lipidol.* **2005**, *16* (3), 301−6.
(14) Schlaich, M. P.; Straznicky, N.; Grima, M.; Ika-Sari, C.; Dawood, T.; Mahfoud, F.; Lambert, E.; Chopra, R.; Socratous, F.; Hennebry, S.; Eikelis, N.; Bohm, M.; Krum, H.; Lambert, G.; Esler, M. D.; Sobotka, P. A. Renal denervation: a potential new treatment modality for polycystic ovary syndrome? *J. Hypertens.* **2011**, *29* (5), 991−6.
(15) Whigham, L. D.; Butz, D. E.; Johnson, L. K.; Schoeller, D. A.; Abbott, D. H.; Porter, W. P.; Cook, M. E. Breath carbon stable isotope ratios identify changes in energy balance and substrate utilization in humans. *Int. J. Obes.* **2014**, *38*, 1248−1250.
(16) Lehninger, A.; Nelson, D.; Cox, M. *Lehninger Principles of Biochemistry*, W. H. Freeman, 2008.
(17) Quinn, K. P.; Sridharan, G. V.; Hayden, R. S.; Kaplan, D. L.; Lee, K.; Georgakoudi, I. Quantitative metabolic imaging using endogenous fluorescence to detect stem cell differentiation. *Sci. Rep.* **2013**, *3*, 3432.
(18) Dawson, A. G. Oxidation of cytosolic NADH formed during aerobic metabolism in mammalian cells. *Trends Biochem. Sci.* **1979**, *4* (8), 171−176.
(19) Benson, R. C.; Meyer, R. A.; Zaruba, M. E.; McKhann, G. M. Cellular autofluorescence−is it due to flavins? *J. Histochem. Cytochem.* **1979**, *27* (1), 44−48.
(20) Si, Y.; Yoon, J.; Lee, K. Flux profile and modularity analysis of time-dependent metabolic changes of de novo adipocyte formation. *Am. J. Physiol. Endocrinol. Metab.* **2007**, *292* (6), E1637−1646.
(21) Vander Heiden, M. G.; Cantley, L. C.; Thompson, C. B. Understanding the Warburg effect: the metabolic requirements of cell proliferation. *Science* **2009**, *324* (5930), 1029−1033.
(22) Chance, B.; Williams, G. R. A method for the localization of sites for oxidative phosphorylation. *Nature* **1955**, *176* (4475), 250−254.
(23) Walsh, A. J.; Cook, R. S.; Manning, H. C.; Hicks, D. J.; Lafontant, A.; Arteaga, C. L.; Skala, M. C. Optical metabolic imaging identifies glycolytic levels, subtypes, and early-treatment response in breast cancer. *Cancer Res.* **2013**, *73* (20), 6164−6174.
(24) Ostrander, J. H.; McMahon, C. M.; Lem, S.; Millon, S. R.; Brown, J. Q.; Seewaldt, V. L.; Ramanujam, N. Optical redox ratio differentiates breast cancer cell lines based on estrogen receptor status. *Cancer Res.* **2010**, *70* (11), 4759−4766.
(25) Kirkpatrick, N. D.; Zou, C.; Brewer, M. A.; Brands, W. R.; Drezek, R. A.; Utzinger, U. Endogenous fluorescence spectroscopy of cell suspensions for chemopreventive drug monitoring. *Photochem. Photobiol.* **2005**, *81* (1), 125−134.
(26) Mujat, C.; Greiner, C.; Baldwin, A.; Levitt, J. M.; Tian, F.; Stucenski, L. A.; Hunter, M.; Kim, Y. L.; Backman, V.; Feld, M.; Munger, K.; Georgakoudi, I. Endogenous optical biomarkers of normal and human papillomavirus immortalized epithelial cells. *Int. J. Cancer* **2008**, *122* (2), 363−371.
(27) Maleki, S.; Gopalakrishnan, S.; Ghanian, Z.; Sepehr, R.; Schmitt, H.; Eells, J.; Ranji, M. Optical imaging of mitochondrial redox state in rodent model of retinitis pigmentosa. *J. Biomed. Opt.* **2013**, *18* (1), 16004.
(28) Haviland, J. A.; Tonelli, M.; Haughey, D. T.; Porter, W. P.; Assadi-Porter, F. M. Novel diagnostics of metabolic dysfunction detected in breath and plasma by selective isotope-assisted labeling. *Metabolism* **2012**, *61* (8), 1162−1170.
(29) Risma, K. A.; Hirshfield, A. N.; Nilson, J. H. Elevated Luteinizing Hormone in Prepubertal Transgenic Mice Causes Hyperandrogenemia, Precocious Puberty, and Substantial Ovarian Pathology. *Endocrinology* **1997**, *138* (8), 3540−3547.
(30) Abbott, D. H.; Barnett, D. K.; Bruns, C. M.; Dumesic, D. A. Androgen excess fetal programming of female reproduction: a developmental aetiology for polycystic ovary syndrome? *Hum. Reprod. Update* **2005**, *11* (4), 357−374.
(31) Demissie, M.; Lazic, M.; Foecking, E. M.; Aird, F.; Dunaif, A.; Levine, J. E. Transient prenatal androgen exposure produces metabolic syndrome in adult female rats. *Am. J. Physiol. Endocrinol. Metab.* **2008**, *295* (2), E262−268.
(32) Dumesic, D. A.; Abbott, D. H.; Padmanabhan, V. Polycystic ovary syndrome and its developmental origins. *Rev. Endocr. Metab. Disord.* **2007**, *8* (2), 127−141.
(33) van Houten, E. L.; Kramer, P.; McLuskey, A.; Karels, B.; Themmen, A. P.; Visser, J. A. Reproductive and metabolic phenotype of a mouse model of PCOS. *Endocrinology* **2012**, *153* (6), 2861−2869.
(34) Cruz, G.; Barra, R.; González, D.; Sotomayor-Zárate, R.; Lara, H. E. Temporal window in which exposure to estradiol permanently modifies ovarian function causing polycystic ovary morphology in rats. *Fertil. Steril.* **2012**, *98* (5), 1283−1290.
(35) Rosa, E. S. A.; Guimaraes, M. A.; Padmanabhan, V.; Lara, H. E. Prepubertal administration of estradiol valerate disrupts cyclicity and leads to cystic ovarian morphology during adult life in the rat: role of sympathetic innervation. *Endocrinology* **2003**, *144* (10), 4289−4297.
(36) Sotomayor-Zarate, R.; Dorfman, M.; Paredes, A.; Lara, H. E. Neonatal exposure to estradiol valerate programs ovarian sympathetic innervation and follicular development in the adult rat. *Biol. Reprod.* **2008**, *78* (4), 673−680.
(37) Chapman, J. C.; Min, S. H.; Freeh, S. M.; Michael, S. D. The estrogen-injected female mouse: new insight into the etiology of PCOS. *Reprod. Biol. Endocrinol.* **2009**, *7*, 47.
(38) Agarwal, A. R.; Zhao, L.; Sancheti, H.; Sundar, I. K.; Rahman, I.; Cadenas, E. Short-term cigarette smoke exposure induces reversible changes in energy metabolism and cellular redox status independent of inflammatory responses in mouse lungs. *Am. J. Physiol.* **2012**, *303* (10), L889−898.
(39) Ghanian, Z.; Maleki, S.; Reiland, H.; Butz, D. E.; Chiellini, G.; Assadi-Porter, F. M.; Ranji, M. Optical imaging of mitochondrial redox state in rodent models with 3-iodothyronamine. *Exp Biol. Med. (London, U.K.)* **2014**, *239* (2), 151−158.
(40) Ward, J. H. Hierarchical Grouping to Optimize an Objective Function. *J. Am. Stat. Assoc.* **1963**, *58* (301), 236−244.
(41) Xia, J.; Sinelnikov, I. V.; Han, B.; Wishart, D. S. MetaboAnalyst 3.0—making metabolomics more meaningful. *Nucleic Acids Res.* **2015**, DOI: 10.1093/nar/gkv380.
(42) Ewens, K. G.; Stewart, D. R.; Ankener, W.; Urbanek, M.; McAllister, J. M.; Chen, C.; Baig, K. M.; Parker, S. C.; Margulies, E. H.; Legro, R. S.; Dunaif, A.; Strauss, J. F., 3rd; Spielman, R. S. Family-based analysis of candidate genes for polycystic ovary syndrome. *J. Clin. Endocrinol. Metab.* **2010**, *95* (5), 2306−2315.

DOI: 10.1021/acs.jproteome.5b00307
J. Proteome Res. 2015, 14, 3284−3291

(43) Wu, G. Amino acids: metabolism, functions, and nutrition. *Amino Acids* **2009**, *37* (1), 1−17.
(44) Newgard, C. B.; An, J.; Bain, J. R.; Muehlbauer, M. J.; Stevens, R. D.; Lien, L. F.; Haqq, A. M.; Shah, S. H.; Arlotto, M.; Slentz, C. A.; Rochon, J.; Gallup, D.; Ilkayeva, O.; Wenner, B. R.; Yancy, W. S., Jr.; Eisenson, H.; Musante, G.; Surwit, R. S.; Millington, D. S.; Butler, M. D.; Svetkey, L. P. A branched-chain amino acid-related metabolic signature that differentiates obese and lean humans and contributes to insulin resistance. *Cell Metab.* **2009**, *9* (4), 311−326.
(45) Adams, S. H. Emerging perspectives on essential amino acid metabolism in obesity and the insulin-resistant state. *Adv. Nutr.* **2011**, *2* (6), 445−456.
(46) Young, G. A. Amino acids and the kidney. *Amino Acids* **1991**, *1* (2), 183−192.
(47) Atiomo, W.; Daykin, C. A. Metabolomic biomarkers in women with polycystic ovary syndrome: a pilot study. *Mol. Hum. Reprod.* **2012**, *18* (11), 546−553.
(48) Zhao, Y.; Fu, L.; Li, R.; Wang, L. N.; Yang, Y.; Liu, N. N.; Zhang, C. M.; Wang, Y.; Liu, P.; Tu, B. B.; Zhang, X.; Qiao, J. Metabolic profiles characterizing different phenotypes of polycystic ovary syndrome: plasma metabolomics analysis. *BMC Med.* **2012**, *10*, 153.
(49) Sochor, M.; Baquer, N. Z.; McLean, P. Regulation of pathways of glucose metabolism in kidney. The effect of experimental diabetes on the activity of the pentose phosphate pathway and the glucuronate-xylulose pathway. *Arch. Biochem. Biophys.* **1979**, *198* (2), 632−646.
(50) Grant, C. M. Metabolic reconfiguration is a regulated response to oxidative stress. *J. Biol.* **2008**, *7* (1), 1.
(51) Kruger, N. J.; von Schaewen, A. The oxidative pentose phosphate pathway: structure and organisation. *Curr. Opin. Plant Biol.* **2003**, *6* (3), 236−246.
(52) Juhnke, H.; Krems, B.; Kotter, P.; Entian, K. D. Mutants that show increased sensitivity to hydrogen peroxide reveal an important role for the pentose phosphate pathway in protection of yeast against oxidative stress. *Mol. Gen. Genet.* **1996**, *252* (4), 456−464.
(53) Peterson, D. T.; Greene, W. C.; Reaven, G. M. Effect of experimental diabetes mellitus on kidney ribosomal protein synthesis. *Diabetes* **1971**, *20* (10), 649−654.
(54) Spiro, R. G. Search for a biochemical basis of diabetic microangiopathy. *Diabetologia* **1976**, *12* (1), 1−14.
(55) Mogensen, C. E.; Andersen, M. J. Increased kidney size and glomerular filtration rate in untreated juvenile diabetes: normalization by insulin-treatment. *Diabetologia* **1975**, *11* (3), 221−224.
(56) Pritsos, C. A. Cellular distribution, metabolism and regulation of the xanthine oxidoreductase enzyme system. *Chem.-Biol. Interact.* **2000**, *129* (1−2), 195−208.
(57) Racasan, S.; Turkstra, E.; Joles, J. A.; Koomans, H. A.; Braam, B. Hypoxanthine plus xanthine oxidase causes profound natriuresis without affecting renal blood flow autoregulation. *Kidney Int.* **2003**, *64* (1), 226−231.
(58) Azziz, R. How prevalent is metabolic syndrome in women with polycystic ovary syndrome? *Nat. Clin. Pract. Endocrinol. Metab.* **2006**, *2* (3), 132−133.
(59) Wamelink, M. M.; Struys, E. A.; Jakobs, C. The biochemistry, metabolism and inherited defects of the pentose phosphate pathway: a review. *J. Inherited Metab. Dis.* **2008**, *31* (6), 703−717.
(60) Hatefi, Y. The mitochondrial electron transport and oxidative phosphorylation system. *Annu. Rev. Biochem.* **1985**, *54*, 1015−1069.
(61) Singer, T. P.; Kearney, E. B.; Zastrow, N. Isolation and properties of succinic dehydrogenase. *Biochim. Biophys. Acta* **1955**, *17* (1), 154−155.
(62) Lin, S. J.; Guarente, L. Nicotinamide adenine dinucleotide, a metabolic regulator of transcription, longevity and disease. *Curr. Opin. Cell Biol.* **2003**, *15* (2), 241−246.
(63) Georgakoudi, I.; Quinn, K. P. Optical imaging using endogenous contrast to assess metabolic state. *Annu. Rev. Biomed. Eng.* **2012**, *14*, 351−67.
(64) Skala, M. C.; Riching, K. M.; Gendron-Fitzpatrick, A.; Eickhoff, J.; Eliceiri, K. W.; White, J. G.; Ramanujam, N. In vivo multiphoton microscopy of NADH and FAD redox states, fluorescence lifetimes, and cellular morphology in precancerous epithelia. *Proc. Natl. Acad. Sci. U.S.A.* **2007**, *104* (49), 19494−19499.
(65) Rice, W. L.; Kaplan, D. L.; Georgakoudi, I. Two-photon microscopy for non-invasive, quantitative monitoring of stem cell differentiation. *PLoS One* **2010**, *5* (4), e10075.
(66) Kobayashi, K.; Neely, J. R. Control of maximum rates of glycolysis in rat cardiac muscle. *Circ. Res.* **1979**, *44* (2), 166−175.
(67) Papandreou, I.; Cairns, R. A.; Fontana, L.; Lim, A. L.; Denko, N. C. HIF-1 mediates adaptation to hypoxia by actively downregulating mitochondrial oxygen consumption. *Cell Metab.* **2006**, *3* (3), 187−197.
(68) Mayevsky, A.; Zarchin, N.; Friedli, C. M. Factors affecting the oxygen balance in the awake cerebral cortex exposed to spreading depression. *Brain Res.* **1982**, *236* (1), 93−105.
(69) Vercesi, A. E.; Castilho, R. F.; Kowaltowski, A. J.; Oliveira, H. C. Mitochondrial energy metabolism and redox state in dyslipidemias. *IUBMB Life* **2007**, *59* (4−5), 263−268.

DOI: 10.1021/acs.jproteome.5b00307
J. Proteome Res. 2015, 14, 3284−3291